1521-009X/51/1/8–16$35.00
DRUG METABOLISM AND DISPOSITION

dx.doi.org/10.1124/dmd.122.001019
Drug Metab Dispos 51:8–16, January 2022

Covalent Binding Mechanism of Furmonertinib and Osimertinib With Human Serum Albumin[S]

Yali Wu, Lili Chen, Jian Chen, Hao Xue, Qingfeng He, Dafang Zhong, and Xingxing Diao

State Key Laboratory of Drug Research, Shanghai Institute of Materia Medica, Chinese Academy of Sciences, Shanghai, China (Y.W., L.C., H.X., D.Z., X.D.); University of Chinese Academy of Sciences, Beijing, China (Y.W., L.C., D.Z., X.D.); Radiopharmacy and Molecular Imaging Center (J.C.), and Department of Clinical Pharmacy and Pharmacy Administration (Q.H.), School of Pharmacy, Fudan University, Shanghai, China; and Key Laboratory of Smart Drug Delivery (Fudan University), Ministry of Education, Shanghai, China(J.C.)

Received July 2, 2022; accepted October 14, 2022

ABSTRACT

As third-generation tyrosine kinase inhibitors, furmonertinib and osimertinib exhibit better efficacy than first- and second-generation tyrosine kinase inhibitors in patients with advanced non-small cell lung cancer. However, radioactive pharmacokinetics studies showed that parent-related components remain in human plasma for at least 21 days after oral administration. Similar pharmacokinetic profiles were found in pyrotinib and neratinib, which have been identified to covalently bind with human serum albumin at Lys-190, leading to low extraction recovery in protein precipitation. However, the binding mechanism of furmonertinib and osimertinib in human plasma has not been confirmed. Comprehensive techniques were used to investigate the mechanism of this binding, including ultra high-performance liquid chromatography coupled with high-resolution mass spectrometry and online/offline radioactivity profiling. SDS–PAGE and further autoradiography were also used to detect drug-protein adducts. We found that most furmonertinib exists in the human plasma following ex vivo incubation in the form of protein-drug adducts. Only lysine-furmonertinb adducts were found in pronase digests. A standard reference of lysine-furmonertinib was synthesized and confirmed by NMR. Through peptide mapping analysis, we confirmed that furmonertinib almost exclusively binds with human serum albumin (HSA) in plasma following ex vivo incubation, via Michael addition at Lys-195 and Lys-199, instead of Lys-190. Two peptides found to bond with furmonertinib were ASSAKQR and LKCASLQK. Osimertinib was also found to bond with Lys-195 and Lys-199 of HSA via peptide mapping analysis.

SIGNIFICANCE STATEMENT

Here we report that furmonertinib and osimertinib can covalently bind with human serum albumin at the site of Lys-195 and Lys-199 instead of Lys-190, potentially leading to the long duration of drug-protein adducts in the human body.

Introduction

Protein kinases are involved in the pathogenesis and progression of many illnesses, especially cancer-related diseases. Over 40 protein kinases have been developed as drug targets, with candidate chemicals undergoing clinical trials (Fischer, 2017; Bhullar et al., 2018; Carles et al., 2018).

Osimertinib, as a third-generation epidermal growth factor receptor (EGFR) tyrosine kinase inhibitor (TKI), is effective in patients with acquired resistance to first-generation TKIs and has been a first-line EGFR TKI option to treat patients with advanced non-small cell lung cancer (NSCLC) (Herbst et al., 2018; Ramalingam et al., 2018). However, radioactivity pharmacokinetic studies revealed that osimertinib-related components remained high until 84 days post-administration (Wu et al., 2021). Furmonertinib, with a classic acrylamide warhead, is a newly developed third-generation EGFR TKI to treat patients with NSCLC developed by Shanghai Allist Pharmaceuticals Co., Ltd. It also can bind with proteins in human plasma, resulting in low unbound drug concentrations. After the oral administration of 97.9 μCi/81.5 mg [^{14}C] furmonertinib mesylate to healthy male volunteers, the sum of the areas under the curve of furmonertinib and its major metabolite AST5902 accounted for less than 3% of the total plasma radioactivity (Fig. 1). Meng et al., (2022), Wang et al. (2010), and Liu et al. (2010) found that most TKIs can covalently bind to Lys-190 of human serum albumin (HSA) via Michael addition. However, for osimertinib and furmonertinib, Liu et al. (2010) only found drug-protein adducts through an intact protein analysis and a drug-amino acid adduct analysis through HCl hydrolysis, in which case the main binding component is obscure. Additionally, whether there are other binding sites is still unknown. Neratinib and pyrotinib can only bind with human serum albumin, while for osimertinib and furmonertinib, they can strongly bind with rat and mouse serum albumin as well (Liu et al., 2020). As comprehensive evidence has proved that neratinib and pyrotinib mainly bind with Lys-190 in human serum albumin (Wang et al., 2010; Meng et al., 2019), which does not exist in rat and mouse serum

The study was partially financially supported by a grant from the National Natural Science Foundation of China [Grant 81903701].

No author has an actual or perceived conflict of interest with the contents of this article.

https://doi.org/10.1124/dmd.122.001019.

[S] This article has supplemental material available at dmd.aspetjournals.org.

ABBREVIATIONS: ALK, anaplastic lymphoma kinase; DBU, 1,8-diazabicyclo[5.4.0]undec-7-ene; DCM, dichloromethane; DMAP, 4-dimethylaminopyridine; EGFR, epidermal growth factor receptors; HRMS, high-resolution mass spectrometry; HSA, human serum albumin; MS, mass spectrometry; NSCLC, non-small cell lung cancer; PD, pharmacodynamic; PK, pharmacokinetic; SEC, size exclusion chromatography; TCEP, Tris(2-carboxyethyl) phosphine; TKI, tyrosine kinase inhibitor; VEGFR, vascular endothelial growth factor receptors.

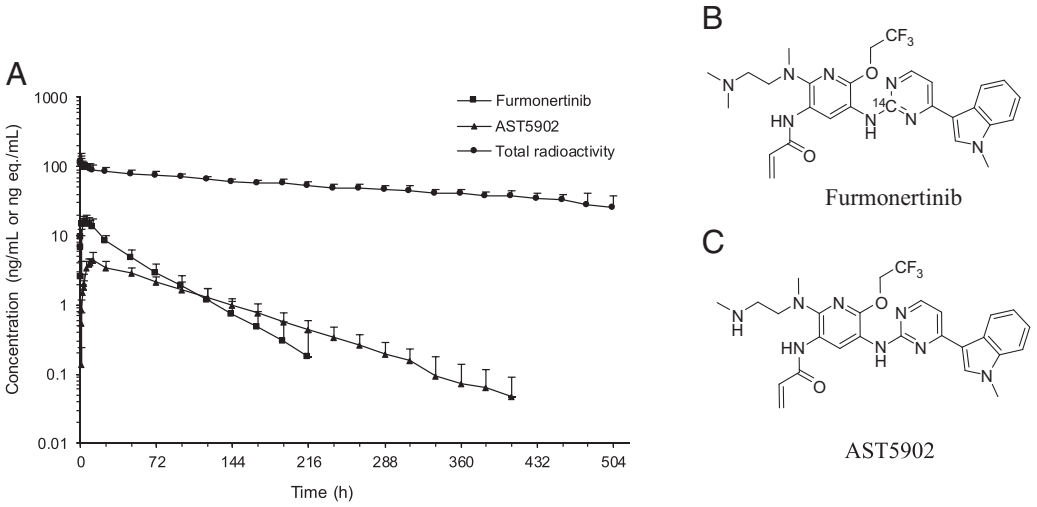

Fig. 1. (A) Time-concentration (radioactivity) profile of furmonertinib in human plasma after oral administration of 97.9 μCi/81.5 mg [^{14}C] furmonertinib mesylate to healthy male volunteers (Meng et al., 2022); (B) structure of furmonertinib; (C) structure of the main metabolite AST5902.

albumin, it is possible that osimertinib and furmonertinib, have other binding sites in human plasma which also exist in rat and mouse.

Various technologies have been used in the identification and characterization of drug-protein adducts in this article. Separation methods such as gel electrophoresis and liquid chromatography (LC) are widely applied. High-resolution mass spectrometry help give the information about both intact adducts and digested peptides. In this study, we used [^{14}C]-radiolabeled furmonertinib and osimertinib labeled with stable isotopes to investigate the exact binding site of drug-protein adducts.

Material and Methods

Materials

[^{14}C] Furmonertinib was synthesized by the Shanghai Qizhen Radiosynthesis Research Center (Shanghai, China), and furmonertinib was obtained from Shanghai Allist Pharmaceuticals Inc. (Shanghai, China), while osimertinib and osimertinib-d9 were obtained from MedChemExpress Co., Ltd (Monmouth Junction, NJ, USA). Ammonium acetate, 1,8-diazabicyclo[5.4.0]undec-7-ene (DBU), 4-dimethyl aminopyridine (DMAP) and dichloromethane (DCM) were purchased from Sinopharm (Shanghai, China). Acetonitrile, trypsin, and human serum albumin were provided by Sigma–Aldrich Co., Ltd. (St. Louis, Missouri, USA), while formic acid was purchased from Rhawn (Shanghai, China). Pronase was obtained from Roche Inc. (Mannheim, Germany), and human plasma (Asian, mixed-sex, $n > 30$) was obtained from The Third Affiliated Hospital of Qiqihar Medical University (Qiqihar, China). PBS, Tris(2-carboxyethyl) phosphine (TCEP), iodoacetamide, and Coomassie brilliant blue G250 were provided by Meilun Biotechnology (Dalian, China). Boc-lysine was purchased from GL Biochem Ltd. (Shanghai, China). Fifteen-milliliter Millipore centrifugal filter devices were obtained from Merck KGaA (Darmstadt, Germany). The Milli-Q system (Molsheim, France) was used to prepare deionized H_2O.

Methods

Size Exclusion Chromatography Separation of Human Plasma-Furmonertinib Adducts. [^{14}C] furmonertinib and non-radiolabeled furmonertinib were incubated with human plasma at a final concentration of 10 μg/ml. At time points 0, 2, 4, and 20 hours, the samples were collected and separated on a Zenix SEC-150 column (7.8×300 mm, 3 μm, Sepax Technologies, Inc. Ltd., Suzhou, China) using a Vanquish ultrahigh-performance liquid chromatography (UPLC) system (Thermo Fisher Scientific, MA, USA) coupled with an online radioactive flow detector β-RAM (LabLogic System Ltd., Sheffield, UK) using the following method: the mobile phase was 50 mM ammonium acetate with 30% acetonitrile, the column temperature was set at 25°C, and the flow rate was 0.5 ml/min, separated for 75 minutes.

Pronase Digestion. The effluent from size exclusion chromatography (SEC) separation with radioactive components was collected in tubes for further investigation. It was concentrated and desalted using Amicon Ultra 15 ml centrifugal filters (10K, Millipore), and the drug-protein adducts were reconstituted using 50 mM ammonium bicarbonate. Pronase was prepared by deionized water in a 20 mg/ml stock solution. The reconstituted protein samples were digested by pronase at a final concentration of 2 mg/ml enzyme. The digested solution was analyzed by UPLC-β-RAM and UPLC-high-resolution mass spectrometry (HRMS) with an HSS T3 C18 column (100 × 2.1 mm, 1.8 μm; Waters, MA, USA) at 40°C. The flow rate was 0.3 ml/ml, and the mobile phase was 0.1% water (A) with 0.1% acetonitrile (B). The first 3 minutes of UPLC flow was equilibrated with 2% B and then linearly increased to 95% B in the following 17 minutes, before being held for 1 minute and quickly returning to 2% B in 0.5 minutes, followed by 3.5 minutes of equilibrium.

Synthesis, Purification, and Identification of the Furmonertinib-Lysine Reference Standard. To a solution of Boc-Lys-OH (45 mg, 0.18 mmol) in acetonitrile, DBU (83 mg, 0.54 mmol), and DMAP (5 mg, 0.04 mmol) was added at room temperature under a nitrogen atmosphere, followed by furmonertinib (30 mg, 0.045 mmol). The resulting mixture was stirred at 80°C overnight. The formation of furmonertinib Boc-Lys-OH was confirmed by monitoring the $[M+H]^+$ at m/z 814 via liquid chromatography–mass spectrometry.

Furmonertinib Boc-Lys-OH (27 mg, 0.033 mmol) was dissolved in 4 ml of DCM, and 400 μl of formic acid was added. The mixture was stirred at room temperature for 30 minutes. Once completed, the solvent was removed under a vacuum. The resulting crude product was purified on a semi-prep HPLC column (C18, 150 × 21.2 mm, 5 μm). Mobile phase A was acetonitrile, and mobile phase B comprised 0.1% formic acid in water. The mobile phase flow rate was 10 ml/min, and the mobile phase gradient was as follows: mobile phase A was started at 10% and held for 5 minutes, and then increased to 90% over 60 minutes in a linear manner. The target product peaked at approximately 23 minutes, and the fraction containing the furmonertinib-lysine adduct was identified by monitoring $[M+H]^+$ at m/z 714 by liquid chromatography–mass spectrometry. The fraction was concentrated under a vacuum to collect furmonertinib-lysine adducts and then dried using a freeze dryer. The product was further confirmed via NMR analysis and high-resolution mass spectrometry.

Intact Protein Analysis. [^{12}C] furmonertinib and [^{14}C] furmonertinib were first prepared at 1 mg/ml (^{12}C/^{14}C is 1:1) in methanol as working solutions. Then, 10 μl of the cold/hot working solution were mixed with 80 μl of human plasma and further diluted with 900 μl of PBS. The mixture was incubated at 37°C for 36 hours. The sample was centrifuged at 15000 rpm for 10 minutes before being applied to the liquid chromatography–tandem mass spectrometry system. Proteins were separated on an ACQUITY UPLC Protein BEH C4 column (300 Å, 1.7 μm, 2.1 mm×50 mm). The mobile phase was 0.1% formic acid water (A) and 0.1% formic acid acetonitrile (B) with a flow rate of 0.3 ml/min, and the column temperature was set at 80°C. In the first minute, the column was equilibrated with 2% B and then linearly increased to 50% B in the following 6 minutes, holding for 1 minute and quickly returning to 2% B in 0.5 minute, followed by 1.5 minutes of equilibrium. The settings for the Q Exactive Plus Hybrid Quadrupole Orbitrap Mass Spectrometer (Thermo Fisher Scientific, MA, USA) were as follows: capillary temperature, 320°C; spray voltage, 3800; sheath gas, 35; and aux gas, 10. Full-scan mass spectra were acquired with a resolution of

70000 and a mass range from 150 to 2000. The mass spectra data were analyzed with Biopharma Finder software 4.0 (Thermo Fisher Scientific, MA, USA).

SDS–PAGE and Autoradiography. The incubation sample for intact protein analysis was used for SDS-gel separation and radioactivity profiling. The plasma incubation samples were mixed with a loading buffer, incubated at 95°C for 10 minutes, and then separated by 10% SDS–PAGE gel. Electrophoresis was performed by applying a constant voltage of 60 V for 30 minutes followed by a voltage of 120 V for the stacking gel for 2 hours in an ice bath to separate the plasma components. After electrophoresis, the gel was cut off and stained by soaking with a Coomassie stain solution for 30 minutes with shaking. The gel was destained by soaking in 30% methanol and 10% formic acid for 24 hours. The gel was applied to a GenoSens 1850 Gel Doc System (Clinx, Shanghai, China) to detect the proteins in plasma. Then the gel was soaked in 10% glycerin plus 20% anhydrous ethanol and dried at 60°C for autoradiography. The dried gel was applied to a PerkinElmer storage phosphor system to obtain the radioactivity profile.

In-Gel Digestion, Peptide Mapping, and Off-Line Radio-Profiling. For furmonertinib-protein adducts, the radioactive gel band was cut into 1mm×1mm pieces and washed with a destaining solution (50 mM ammonium bicarbonate) at 37°C for 30 minutes with shaking 3 times. Then, the liquid was discarded, and 10% TCEP was added to the samples as a reducing buffer at 60°C for 10 minutes. The samples were allowed to cool, and then the buffer was discarded. Then, 100 mM iodoacetamide was added as an alkylation buffer in the dark at room temperature for 1 hour. The gels were washed twice with a destaining solution at 37°C for 15 minutes with shaking. Acetonitrile was incubated with the gel for 10 minutes at room temperature and then carefully removed to allow the gels to dry for 10 minutes. Then, 10 μg/ml sequencing grade trypsin was added to the dried gel at an enzyme protein ratio of 1:45 (*w:w*) at 30°C overnight. The mixture was transferred to a clean tube, and 1% formic acid was added to stop the enzyme digestion. Peptides were separated on an ACQUITY PREMIER Peptide CSH C18 column (130 Å, 1.7 μm, 2.1 mm×150 mm) and analyzed via HRMS and an offline radioactive detector. The mobile phase was 0.1% formic acid water (A) and 0.1% formic acid acetonitrile (B) with a flow rate of 0.3 ml/min. The column temperature was set to 60°C. In the first 3 minutes, the column was equilibrated with 2% B, linearly increased to 45% B in the following 72 minutes, linearly increased to 95% B in the following 5 minutes, held for 10 minutes and quickly returned to 2% B in 0.3 minutes, followed by 7.7 minutes of equilibrium. The tuning method for the Q Exactive Plus Hybrid Quadrupole Orbitrap Mass Spectrometer was the same as that used in the intact protein analysis. Full-scan mass spectra were acquired with resolution at 70000 and a mass range from 200 to 2000. The settings for data-dependent MS^2 were as follows: resolution, 17500; scan range, from 200 to 2000; and normalized collision energy, 27%. The mass spectra data of peptide mapping were analyzed using Biopharma Finder software 4.0. The same samples were also injected into UPLC coupled with a fraction collector (ASX-280-FC, Thermo Fisher Scientific, MA, USA) with the same LC system and methods. Deepwell LumaPlate 96-well plates (Perkin Elmer, MA, USA) were used to collect the eluent. The plates were dried at room temperature and read using a Hidex Sense Beta microplate reader (Hidex, Turku, Finland), and the final radioactivity profile was integrated by Radiochromatography Data Collection and Analysis Software Laura (LabLogic Systems Ltd., Sheffield, United Kingdom). For non-radiolabeled osimertinib, 10 μl of the osimertinib/d9-osimertinib working solution was mixed with 80 μl of human plasma and further diluted with 900 μl of PBS. The mixture was incubated at 37°C for 36 hours. Then the incubation sample was pretreated the same as furmonertinib described before. The in-gel digestion sample of osimertinib-protein adducts were analyzed the same as mentioned before.

Data Analysis

The mass spectral data were acquired using Xcalibur software. Scan filters were employed to obtain the extracted ion chromatogram within a 5 ppm mass tolerance. Intact protein analysis and peptide mapping were performed with Biopharma Finder software 4.0 using the already known sequence of human serum albumin. In the peptide mapping analysis, the software was configured to have carbamidomethylation (+57.021 Da) as a regular cysteine modification. The variable modification was set for a lysine modification of +568.2522 Da (molecular mass of furmonertinib).

Results

SEC Separation and Online Radioactive Profiling

Human plasma incubated with [^{14}C] furmonertinib and non-radiolabeled furmonertinib was injected directly into ultra high-performance liquid chromatography coupled with an online β-RAM detector. The sample was separated with an SEC column. The radioactivity profiles of 0-hour, 2-hour, 4-hour, and 20-hour incubations are shown in Fig. 2. The single radioactive peak of [^{14}C] furmonertinib was observed in the 0-hour incubation sample in Fig. 2A, whereas another radioactive peak was observed between 10 and 12 minutes in the samples incubated for 2 hours, 4 hours, and 20 hours, as shown in Fig. 2, B–D. In this case, the single peak of the radioactive protein-drug adduct suggested the likelihood of mainly 1 plasma protein covalently binding with furmonertinib. The eluent of the main radioactive peak was collected with a few injections for further investigation.

Pronase Digestion of Furmonertinib-Plasma Protein Adducts

The radioactive eluent collected from SEC separation was desalted and concentrated with 50 mM ammonium bicarbonate for pronase digestion. The digestion sample was then analyzed via ultra high-performance liquid chromatography coupled with an online β-RAM detector and HRMS detector using the same LC separation method. The radioactivity profile obtained from β-RAM shown in Fig. 3A suggested that furmonertinib binds with sole amino acid in human plasma. At the same retention time, the molecular ion with *m/z* 715.3650 was observed in the full scan, as shown in Fig. 3, B–C. The similar intensity of the isotope peak (*m/z* 717.3683) also confirmed that this eluent is a furmonertinib-related adduct. The MS^2 spectra were also analyzed (Fig. 3D). The fragment with *m/z* 569.2585 was the parent furmonertinib, and ions with *m/z* 670.6047, 524.2008, and 386.1703 were furmonertinib-related fragments.

Structural Identification of the Synthesized Furmonertinib-Lysine Adduct

The synthesized furmonertinib-lysine adducts were determined via NMR (Bruker Avance III 500 NMR spectrometer). The structures and chemical shifts of 1H and 13C of furmonertinib and furmonertinib-lysine are listed in the Supplemental Fig. 1 and Supplemental Table 1. The product ion spectra of the synthesized furmonertinib-lysine standard reference produced by HRMS were used for further determination, as shown in Supplemental Fig. 2. Fragments at *m/z* 670.3072, 587.2963, 524.2016, and 441.1906 were formed from similar cleavages as furmonertinib. The synthesized furmonertinib-lysine was added to the pronase digestion sample, and the extracted ion chromatogram of the ion at *m/z* 715.3650, which represents the furmonertinib-lysine adduct, still shows a single peak with a significant improvement in the mass response (data shown in Supplemental Fig. 3).

Intact Protein Analysis of Drug-Protein Adducts in Human Plasma

Incubation samples of radioactive and non-radiolabeled furmonertinib with human plasma were diluted and injected directly into HRMS to detect intact protein-drug adducts. The deconvolution spectra are shown in Fig. 4A. The measured ion cluster of human serum albumin was 66437 Da. Based on the amino acid sequence acquired from UniProt (https://www.uniprot.org/), considering 17 disulfide bonds formed inside the protein, the theoretical mass of HSA should be 66438 Da. The less abundant ion cluster was 67007 Da, which is 570 Da higher than that of HSA. Considering that the mass value of [^{12}C] furmonertinib was 568 Da and that of [^{14}C] furmonertinib was 570 Da, the error was less than 2 Da, which is tolerable and can be the result of an instrument deviation. The molecular mass of this adduct indicated that the ion cluster 67007 Da was the addition of furmonertinib to HSA.

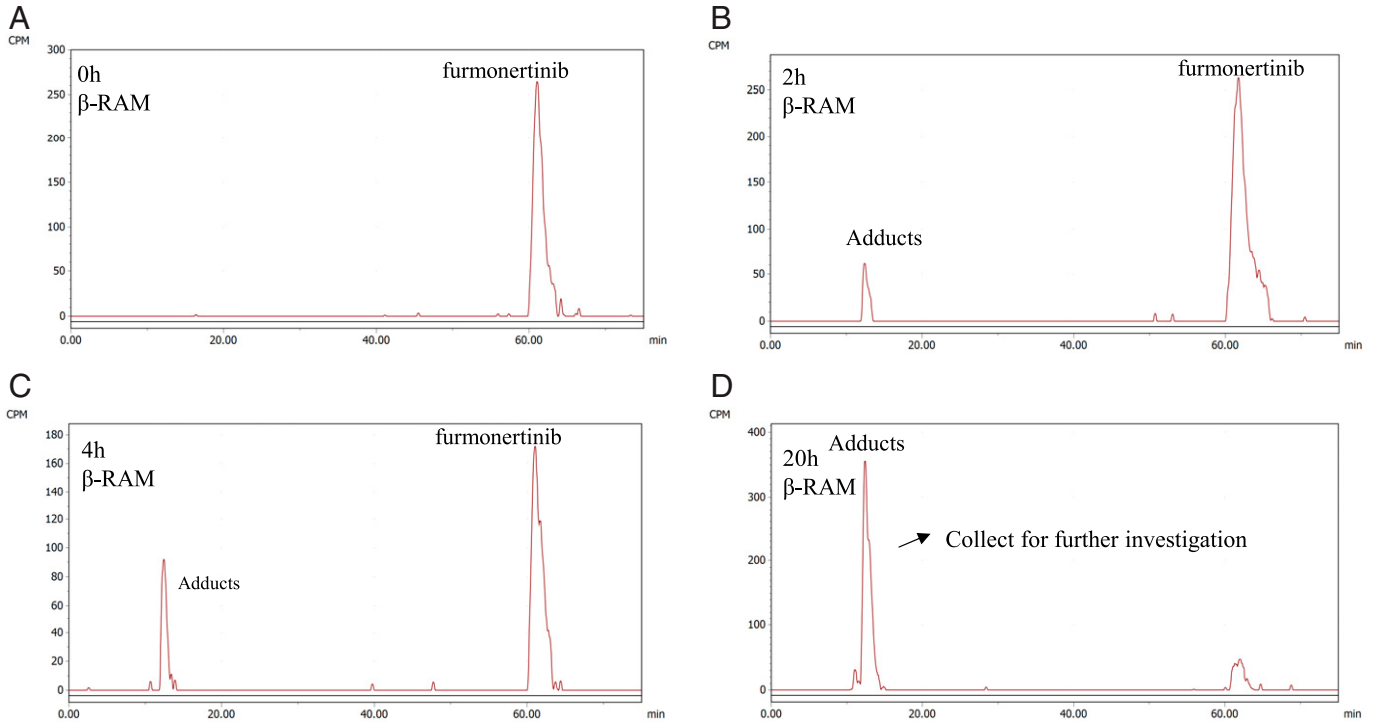

Fig. 2. Radioactivity profiles of SEC separation of [^{14}C] furmonertinib-protein adducts in human plasma incubated with the drug ex vivo.

Radioactivity Profiling of SDS–PAGE Gels and Peptide Mapping

The same radioactive sample of furmonertinib-protein adducts for the intact protein analysis was separated and purified with SDS–PAGE gel for further peptide mapping. The gel was applied to a coomassie blue staining solution and a phosphor imaging plate. The scanning figures are shown in Fig. 4B. The single radioactive protein band between 50 kDa and 70 kDa on the right was cut for further in-gel digestion and peptide mapping. The total ion chromatogram of digests obtained by HRMS is

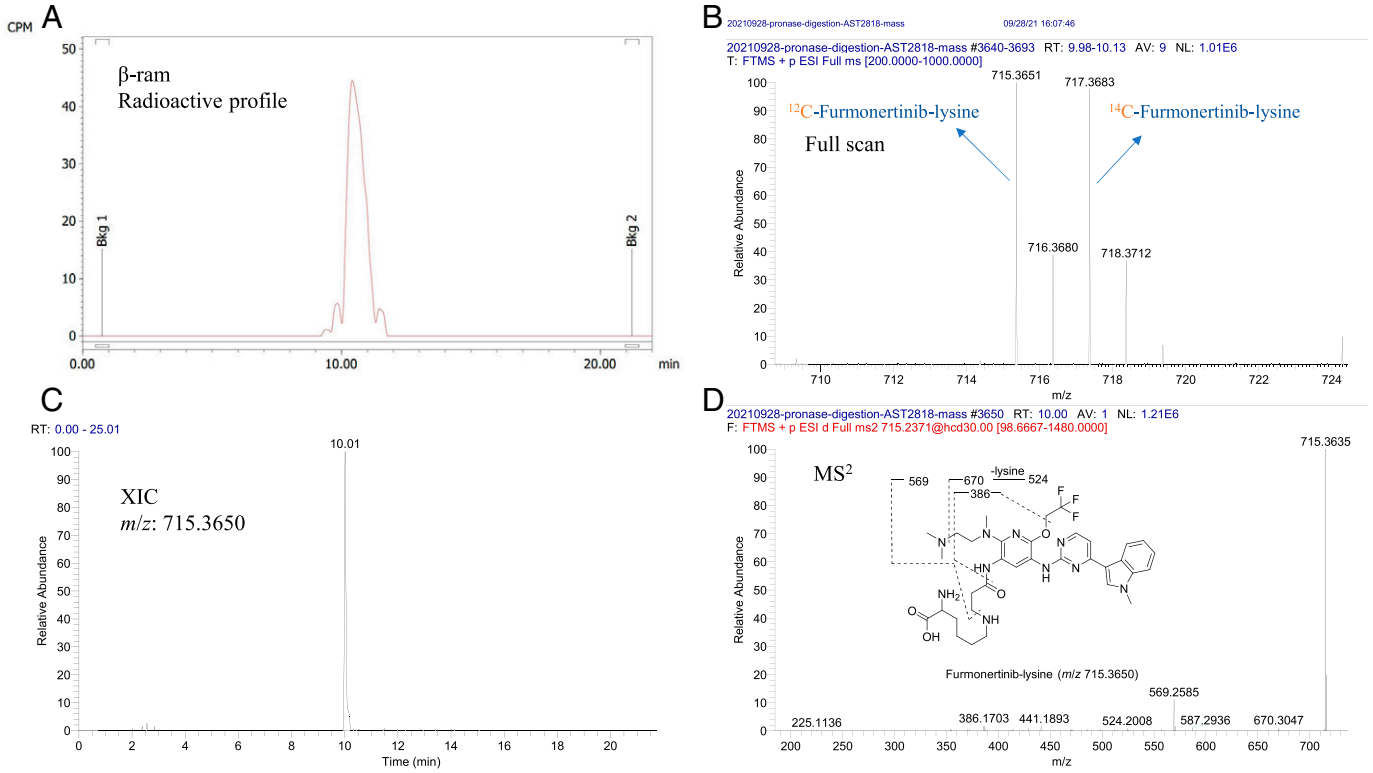

Fig. 3. Pronase digestion of radioactive eluent from SEC separation (A) The radioactive amino acid-small molecular adduct detected with an online β-RAM detector; (B) part of the full MS spectra of the pronase digestion sample obtained with HRMS; (C) the extracted ion spectra of protonated molecular ions at *m/z* 715.3650; (D) the MS2 spectra of protonated molecular ions at *m/z* 715.2371 (<5 ppm)

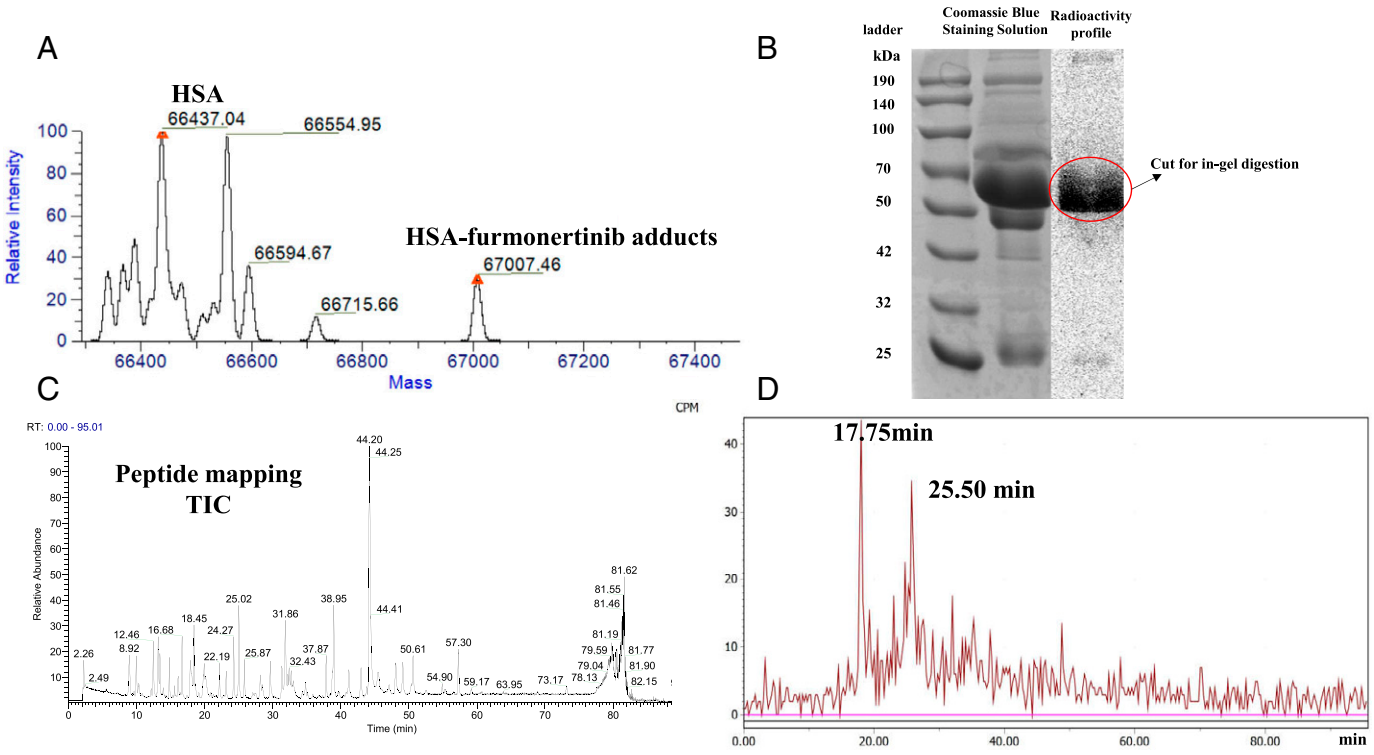

Fig. 4. (A) Deconvolution spectra of the furmonertinib-protein component in human plasma incubated with the drug ex vivo; (B) autoradiography analysis of [^{14}C] furmonertinib-human plasma incubation sample; (C) total ion chromatogram of trypsin-digested incubation sample obtained with HRMS; (D) offline radioactive profile of trypsin-digested incubation sample.

shown in Fig. 4C. The peptide mapping results obtained from Biopharma Finder suggest an 89% coverage of the HSA sequence, confirming that furmonertinib mainly binds with HSA in human plasma. The offline radioactivity profile is shown in Fig. 4D with two main peaks at 17.75 minutes and 25.50 minutes, indicating that two peptides possibly bound to furmonertinib at the lysine of HSA. Non-radiolabeled osimertinib and d9-osimertinib incubation samples were also separated with sodium dodecyl sulfate-polyacrylamide gel electrophoresis as mentioned before.

Identification of the HSA-Drug Binding Site by HRMS

For furmonertinib, two peptide-furmonertinib adducts were detected with HRMS in digests. As shown in Fig. 5A, furmonertinib-ASSAKQR adducts were detected. Peak A represents the [^{12}C] furmonertinib-peptide adduct, while peak B represents the [^{14}C] furmonertinib-peptide. Peak A was an extracted ion chromatogram of *m/z* 439.2262, and peak B was *m/z* 439.8940, both of whose charge states were determined to be 3+. The retention times of peaks A and B were both 18 minutes, which is consistent with that of the offline radioactivity profile in Fig. 4D. For the product ion spectra of these protonated molecular ions, the fragments *m/z* 498.1864 and *m/z* 500.1892 were observed, which represent [MH − $(CH_2)_4NH]^+$ and [^{14}CMH − $(CH_2)_4NH]^+$, respectively, as labeled in Fig. 5A, indicating similar fragmentation in the parent furmonertinib. The doubly protonated ions of [^{12}C] furmonertinib and [^{14}C] furmonertinib were also observed at *m/z* 285.1336 and 286.1337, respectively. The identified y*4+, y*5+, and y*6+ and the corresponding radioactive fragments are also labeled in Fig. 5A. The evidence in Fig. 5A confirmed that furmonertinib can bind to the lysine of peptide ASSAKQR based on the fragmentation pathways and radioactivity profiles.

Similarly, furmonertinib-LKCASLQK adducts were detected at 25 minutes via mass spectrometry (Fig. 5B), consistent with the radioactive results obtained from the offline radioactivity profile. Peak A was an extracted ion chromatogram of *m/z* 505.9341(3^+), while peak B was *m/z* 506.6018(3^+), representing nonradioactive and radioactive adducts, respectively. The ion responses for peak A and peak B in Fig. 5B were almost proportional. The product ion spectra of these two protonated molecular ions are shown. Fragments of [^{12}C] furmonertinib (569.2595) and [^{14}C] furmonertinib (571.2628) were detected to confirm that furmonertinib indeed binds with these peptides. Other identified fragment ions were labeled as well. Finally, the peptide eluent at 25 minutes was identified to be furmonertinib binding with the first lysine of peptide LKCASLQK.

For osimertinib, we intentionally searched for Lys-195-osimertinib and Lys-199-osimertinib adducts. As shown in Fig. 6A, osimertinib-ASSAKQR adducts were detected. Peak A represents the osimertinib-peptide adduct, while peak B represents the d9-osimertinib-peptide adduct. For the product ion spectra of these protonated molecular ions, the fragments *m/z* 429.2033 and *m/z* 432.2220 were observed, which represent [MH − $(CH)_2(CH_3)_2NH]^+$ and [d9MH − $(CH)_2(CD_3)_2NH]^+$, respectively, as labeled in Fig. 6A. The evidence in Fig. 6A confirmed that osimertinib can bind to the lysine of peptide ASSAKQR based on the fragmentation pathways and isotopic characteristics. Also, osimertinib-LKCASLQK adducts were detected at 19 minutes via mass spectrometry (Fig. 6B). Identified fragment ions were labeled as well.

In short, furmonertinib can bind with Lys-195 and Lys-199 of human serum albumin, and these two binding forms are the main forms in humans. The same binding sites are also found in osimertinib-protein adducts.

Discussion

A previous review discussed the binding site between TKIs and HSA, and it seems that Lys-190 of HSA is the binding site for TKIs (Wang et al., 2010; Meng et al., 2019; Liu et al., 2020). However, in our study, through a comprehensive analysis, it was determined that Lys-195 and

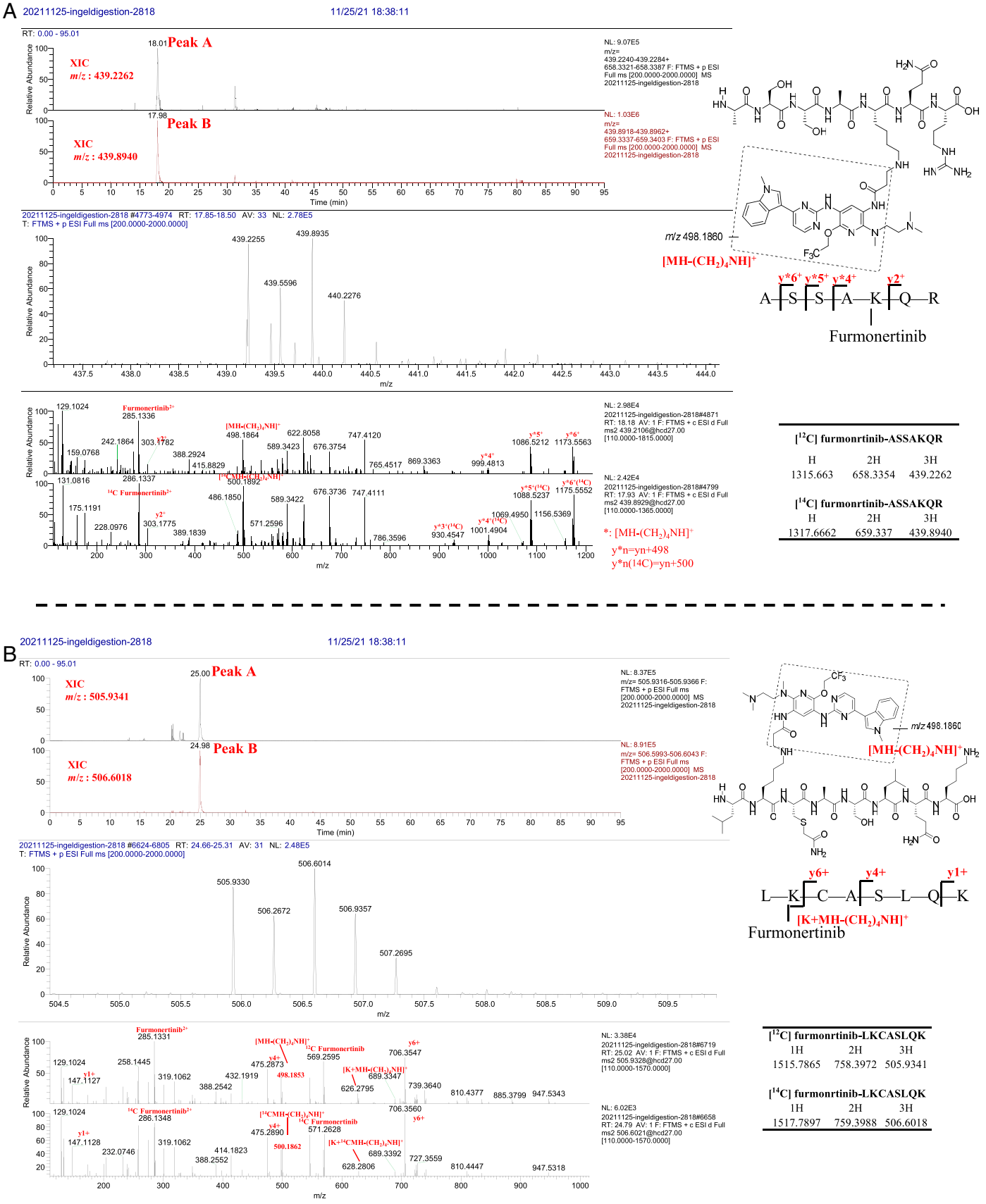

Fig. 5. Structural identification of furmonertinib-ASSAKQR adducts (A) and furmonertinib-LKCASLQK adducts from human plasma incubated with the drug ex vivo (B).

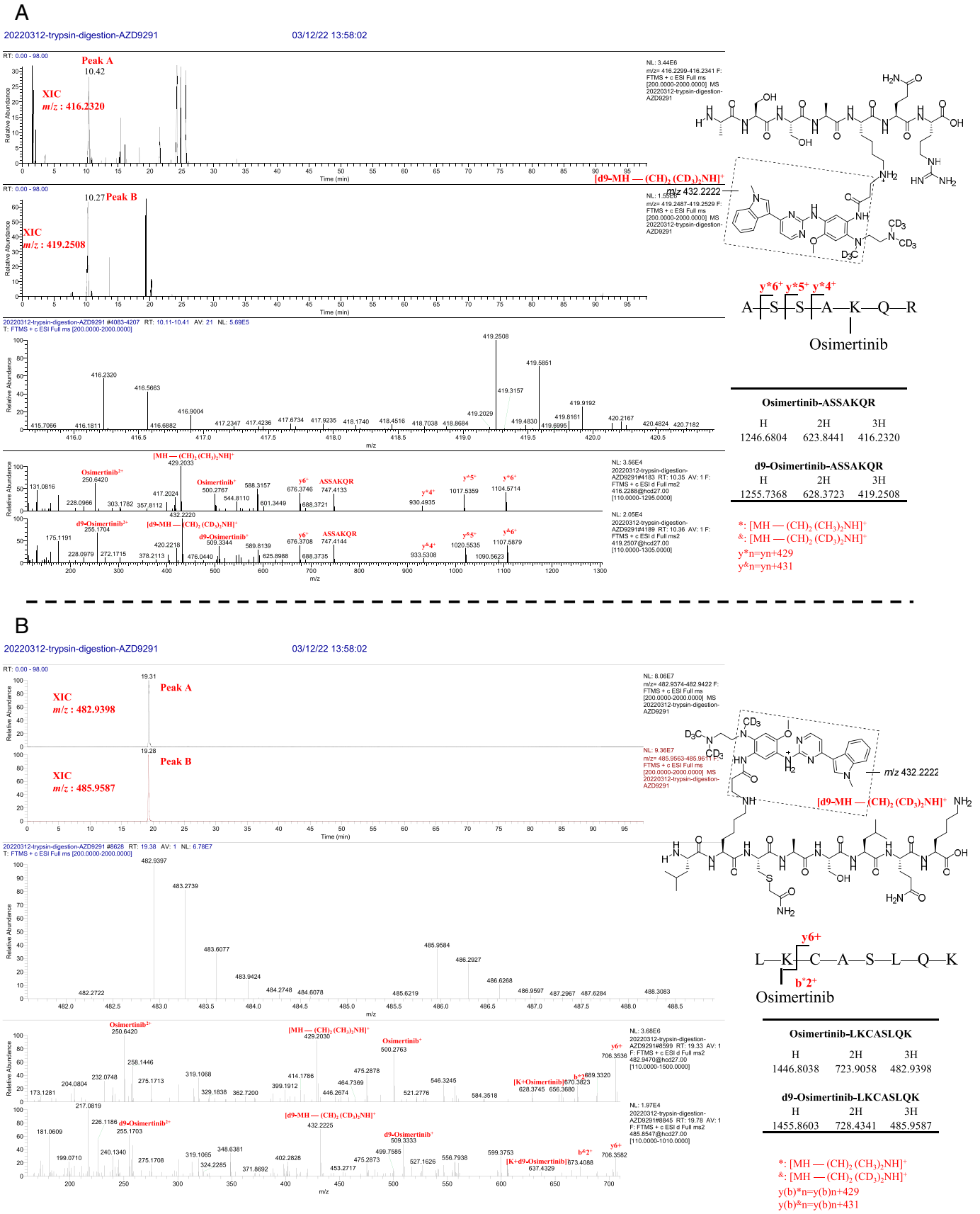

Osimertinib-ASSAKQR

H	2H	3H
1246.6804	623.8441	416.2320

d9-Osimertinib-ASSAKQR

H	2H	3H
1255.7368	628.3723	419.2508

*: [MH — (CH)2 (CH3)2NH]+
&: [MH — (CH)2 (CD3)2NH]+
y*n=yn+429
y&n=yn+431

Osimertinib-LKCASLQK

H	2H	3H
1446.8038	723.9058	482.9398

d9-Osimertinib-LKCASLQK

H	2H	3H
1455.8603	728.4341	485.9587

*: [MH — (CH)2 (CH3)2NH]+
&: [MH — (CH)2 (CD3)2NH]+
y(b)*n=y(b)n+429
y(b)&n=y(b)n+431

Fig. 6. Structural identification of osimertinib-ASSAKQR adducts (A) and osimertinib-LKCASLQK adducts from human plasma incubated with the drug ex vivo (B).

Lys-199 of human serum albumin, instead of Lys-190, bind with furmonertinib and osimertinib following ex vivo incubation.

Advanced Technologies to Detect Drug-Protein Covalent Adducts

Mass spectrometry (MS) is a powerful tool to investigate and characterize the precise chemical structure at the modification site. Instead of analyzing the amino acid one by one using Edman degradation (Walker, 1976), MS can help map the sequence and identify the specific modification. Mass spectrometry-based top-down analysis allows the identification of intact drug-protein adducts, giving the information on molecular mass of adducts. The bottom-up mass spectrometric analysis allows the identification of peptides digested from drug-protein adducts. As described in this article, the protein samples undergo reduction, alkylation, and trypsin (or other proteolytic enzymes) digestion, forming peptides which can be applied to LC-HRMS for structure identification. Various data acquisition methods are used in this context, for example, full-MS scan, data-independent acquisition, data-dependent acquisition, and multiple reaction monitoring.

A limitation of this study is that we performed all incubations ex vivo. Attempts to obtain plasma samples from drug-treated patients for analysis of adduct formation in vivo were unsuccessful. Also, given the relatively low drug concentration in human patient plasma (Cmax around 100 ng eq./ml), it would be difficult to identify the structures of HSA adducts formed in vivo, considering the electrophoretic loss, enzyme digestion efficiency, and relatively low sensitivity of high-resolution mass spectrometry compared with tandem mass spectrometry. Though we have no reason to believe that in vivo adducts and ex vivo adducts could have different structures, further studies to validate the structures of in vivo adducts in human plasma are warranted.

Species Difference

It is not surprising that this type of drug can bind with lysine in the human body since the acrylamide warhead in the structure was designed to bind with the cysteine of the target protein via Michael addition. In our study, through a comprehensive analysis, it was determined that Lys-195 and Lys-199, instead of Lys-190, bind with furmonertinib and osimertinib. Subtle hints can be obtained from the differences in the radioactivity recovery of these compounds in different species. Liu. et al. analyzed the remaining TKIs after incubation with plasma from different species and found that neratinib and pyrotinib only bind with human plasma proteins, while osimertinib and furmonertinib strongly bind with proteins in rat and mouse plasma(Liu et al., 2020). Sequences vary among serum albumin of different species: amino acid residues of 190 to 200 of HSA was KASSAKQRLKC, while for rats, the sequence was VAAVRQRMKC. These 10 amino acid residues locate at a flexible region of HSA at the junction of domains 1 and 2, where have been found to bind with many kinds of drugs, including salicylate, glucose, warfarin, and antibiotics such as benzylpenicillin, piperacillin, amoxicillin, etc(Yvon et al., 1989; Tailor et al., 2016; Yang et al., 2021). We also analyzed the furmonertinib-protein adducts in rat plasma through gel separation and trypsin digestion. Furmonertinib-MKCSSMQR adducts (shown in Supplemental Fig. 4) were identified, which means furmonertinib can bind with Lys-199 of rat serum plasma. However, rat serum albumin does not have Lys-190 and Lys-195 residues, in which case the free drug concentration of the certain electrophilic drug may be distinct among species. For example, the incomplete recovery of neratinib (HKI-272), which was confirmed to bind exclusively with Lys-190 with HSA, was only found in human and monkey serum albumin (Wang et al., 2010). For pyrotinib, which shares a similar core structure with neratinib, was only found to covalently bind with human serum albumin at Lys-190 instead of rat serum albumin, since rat serum albumin only has Lys-199 (Liu et al., 2020). However, in this study, we found that furmonertinib and osimertinib bind with Lys-195 and Lys-199 of HSA instead of Lys-190. Lys-199 residue also exists in rat serum albumin, consistent with the result that these two drugs can strongly bind with both human and rat serum albumin. Interestingly, TKIs are selective in the respect of binding sites with HSA. For TKIs, it is important to deeply investigate the binding mode and site among different species since the free drug concentration in different species could vary vastly. It is vital especially in the first-in-human pharmacokinetic predictions in which case the animal and in vitro data will be incorporated into mathematic models. If the binding behaviors of animal species chosen act significantly different from that of human, fatal mistakes can be made in the predictions for humans.

Safety Concerns

Various biologic outcomes can be triggered by drug-protein adducts, including effects on protein function and activation of innate or adaptive immune systems, causing morbidity and mortality. It should be interesting and important to investigate the potential of covalent binding of TKIs in organs. A wealth of drug-induced liver injuries attributed to chemical reactive metabolites or intermediates formed in vivo biotransformation. For example, the reactive "quinoid" intermediates form from the oxidation of acetaminophen, which can further provide electrophiles that covalently modify functional proteins (Park et al., 2011). It is interesting that, though the electrophilic metabolites of acetaminophen are generated in the liver, the reactive quinone imine metabolite was observed to be covalently bound with hemoglobin, which means that reactive intermediates may migrate from its formation site to the circulation system or even other organs and then subsequently form protein adducts (Axworthy et al., 1988). Additionally, drug-protein adducts that remained in human serum are haptenic complexes that could raise safety concerns regarding hypersensitivity and anaphylaxis. β-lactam antibiotics are perfect examples. The β-lactam structure they have was found to generate adducts with HSA, instigating immune response and causing allergies in patients (Jenkins et al., 2013; Meng et al., 2016). For TKIs, drug–drug interaction caused by HSA needs exceptional attention. Liu et al. assessed the amount of free TKIs released from covalent-plasma proteins adducts, most of which exhibited partial reversibility. If possible, the concentration of free drug and protein adducts in patients can be measured when combination therapy is applied to investigate if any drug substance will interact with the binding between TKIs and plasma protein and further cause a fluctuation of unbound drug concentration.

PK/PD Predictions

The covalent binding between drug and plasma proteins can result in low extraction recovery in pharmacokinetic studies, creating seemingly low absorption. Sometimes, drug components slowly dissociate from adducts, making difficulties for pharmacokinetic (PK) and pharmacodynamic (PD) analysis. Moreover, combination therapies are used for treating NSCLC in the past few years, especially with monoclonal antibodies, considering the inevitably developed resistance from osimertinib (Mancini et al., 2018; Jänne et al., 2022; Vicencio et al., 2022). However, given that TKIs can covalently bind with proteins, whether they would interact with antibodies should also receive attention. The conventional PK/PD studies based on the "free-drug hypothesis" for small molecular drugs have limitations. Unbound (free) drug concentration at the therapeutic target is believed to elicit a pharmacologic effect. For covalent inhibitors, if a modest free drug circulates to the target protein, it will leave abundant protein-drug adducts existing in plasma. Recently, efforts were made to develop methods for covalent drugs in PK/PD studies and the long effect duration of target organs was observed. The detection and quantification of drug-modified protein can help build models to predict the concentrations at target organs, thereby reflecting

the drug effects (Gong et al., 2021). Plasma samples collected can be used for the quantification of peptide-drug adducts, which can be incorporated into PK/PD or PBPK models as biomarkers for further prediction. Previous studies revealed that, mostly, the covalent binding between TKIs and human plasma is reversible, which means HSA can serve as a potential reservoir to maintain the drug effect at the target organ (Liu et al., 2020). Moreover, human has three lysines in the flexible loop region of albumin compared with one for rat and mouse, which may increase free fraction in rodent models in vivo. If a human has a significantly lower free fraction, the clinical efficacy may be negatively impacted.

In conclusion, this study confirmed that furmonertinib and osimertinib mainly covalently bind with HSA in human plasma at the site of Lys-195 and Lys-199, instead of Lys-190, following ex vivo incubation. In general, TKI-HSA adducts could have significant implications in various aspects of drug safety and efficacy; however, in vivo quantitative studies of the adduct levels, adduct half-life, and relative levels of the adducts to the unbound parent drug and unbound metabolites are needed to assess whether the specific adducts detected in this study are relevant. Moreover, if the quantification method of such adducts can be developed and established in the future, adducts can be measured in human patient plasma and the relationship between the adduct level and pharmacodynamics may be investigated.

Authorship Contributions

Participated in research design: Wu, Diao, Zhong.
Conducted experiments: Wu, J. Chen, L.L. Chen.
Contributed new reagents or analytic tools: Wu, L.L. Chen.
Performed data analysis: Wu, Xue, He.
Wrote or contributed to the writing of the manuscript: Wu, Diao, Zhong.

References

Axworthy DB, Hoffmann K-J, Streeter AJ, Calleman CJ, Pascoe GA, and Baillie TA (1988) Covalent binding of acetaminophen to mouse hemoglobin. Identification of major and minor adducts formed in vivo and implications for the nature of the arylating metabolites. *Chem Biol Interact* **68:**99–116.

Bhullar KS, Lagarón NO, McGowan EM, Parmar I, Jha A, Hubbard BP, and Rupasinghe HPV (2018) Kinase-targeted cancer therapies: progress, challenges and future directions. *Mol Cancer* **17:**48.

Carles F, Bourg S, Meyer C, and Bonnet P (2018) PKIDB: A curated, annotated and updated database of protein kinase inhibitors in clinical trials. *Molecules* **23:**908.

Fischer PM (2017) Approved and experimental small-molecule oncology kinase inhibitor drugs: a mid-2016 overview. *Med Res Rev* **37:**314–367.

Gong S, Zhuo Y, Chen S, Hu X, Fan XX, Wu JL, and Li N (2021) Quantification of osimertinib and metabolite-protein modification reveals its high potency and long duration of effects on target organs. *Chem Res Toxicol* **34:**2309–2318.

Herbst RS, Morgensztern D, and Boshoff C (2018) The biology and management of non-small cell lung cancer. *Nature* **553:**446–454.

Jänne PA, Baik C, Su WC, Johnson ML, Hayashi H, Nishio M, Kim DW, Koczywas M, Gold KA, Steuer CE, et al. (2022) Efficacy and safety of patritumab deruxtecan (HER3-DXd) in EGFR inhibitor-resistant, *EGFR*-mutated non-small cell lung cancer. *Cancer Discov* **12:**74–89.

Jenkins RE, Yaseen FS, Monshi MM, Whitaker P, Meng X, Farrell J, Hamlett J, Sanderson JP, El-Ghaiesh S, Peckham D, et al. (2013) β-Lactam antibiotics form distinct haptenic structures on albumin and activate drug-specific T-lymphocyte responses in multiallergic patients with cystic fibrosis. *Chem Res Toxicol* **26:**963–975.

Liu X, Feng D, Zheng M, Cui Y, and Zhong D (2020) Characterization of covalent binding of tyrosine kinase inhibitors to plasma proteins. *Drug Metab Pharmacokinet* **35:**456–465.

Mancini M, Gal H, Gaborit N, Mazzeo L, Romaniello D, Salame TM, Lindzen M, Mahlknecht G, Enuka Y, Burton DG, et al. (2018) An oligoclonal antibody durably overcomes resistance of lung cancer to third-generation EGFR inhibitors. *EMBO Mol Med* **10:**294–308.

Meng J, Liu XY, Ma S, Zhang H, Yu SD, Zhang YF, Chen MX, Zhu XY, Liu Y, Yi L, et al. (2019) Metabolism and disposition of pyrotinib in healthy male volunteers: covalent binding with human plasma protein. *Acta Pharmacol Sin* **40:**980–988.

Meng J, Zhang H, Bao JJ, Chen ZD, Liu XY, Zhang YF, Jiang Y, Miao LY, and Zhong DF (2022) Metabolic disposition of the EGFR covalent inhibitor furmonertinib in humans. *Acta Pharmacol Sin* **43:**494–503.

Meng X, Earnshaw CJ, Tailor A, Jenkins RE, Waddington JC, Whitaker P, French NS, Naisbitt DJ, and Park BK (2016) Amoxicillin and clavulanate form chemically and immunologically distinct multiple haptenic structures in patients. *Chem Res Toxicol* **29:**1762–1772.

Park BK, Boobis A, Clarke S, Goldring CE, Jones D, Kenna JG, Lambert C, Laverty HG, Naisbitt DJ, Nelson S, et al. (2011) Managing the challenge of chemically reactive metabolites in drug development. *Nat Rev Drug Discov* **10:**292–306.

Ramalingam SS, Yang JC, Lee CK, Kurata T, Kim D-W, John T, Nogami N, Ohe Y, Mann H, Rukazenkov Y, et al. (2018) Osimertinib as first-line treatment of EGFR mutation-positive advanced non-small-cell lung cancer. *J Clin Oncol* **36:**841–849.

Tailor A, Waddington JC, Meng X, and Park BK (2016) Mass spectrometric and functional aspects of drug-protein conjugation. *Chem Res Toxicol* **29:**1912–1935.

Vicencio JM, Evans R, Green R, An Z, Deng J, Treacy C, Mustapha R, Monypenny J, Costoya C, Lawler K, et al. (2022) Osimertinib and anti-HER3 combination therapy engages immune dependent tumor toxicity via STING activation in trans. *Cell Death Dis* **13:**274.

Walker JE (1976) Lysine residue 199 of human serum albumin is modified by acetylsalicyclic acid. *FEBS Lett* **66:**173–175.

Wang J, Li-Chan XX, Atherton J, Deng L, Espina R, Yu L, Horwatt P, Ross S, Lockhead S, Ahmad S, et al. (2010) Characterization of HKI-272 covalent binding to human serum albumin. *Drug Metab Dispos* **38:**1083–1093.

Wu Y, Pan L, Chen Z, Zheng Y, Diao X, and Zhong D (2021) Metabolite identification in the preclinical and clinical phase of drug development. *Curr Drug Metab* **22:**838–857.

Yang S, Zhang W, Liu Z, Zhai Z, Hou X, Wang P, Ge G, and Wang F (2021) Lysine reactivity profiling reveals molecular insights into human serum albumin-small-molecule drug interactions. *Anal Bioanal Chem* **413:**7431–7440.

Yvon M, Anglade P, and Wal J-M (1989) Binding of benzyl penicilloyl to human serum albumin. Evidence for a highly reactive region at the junction of domains 1 and 2 of the albumin molecule. *FEBS Lett* **247:**273–278.

Address correspondence to: Dafang Zhong, 501 Haike Road, Shanghai, China 201210. E-mail: dfzhong@simm.ac.cn); or Xingxing Diao, 501 Haike Road, Shanghai, China 201210. E-mail: xxdiao@simm.ac.cn

Drug Metabolism and Disposition

Supplementary material

Covalent binding mechanism of Furmonertinib and Osimertinib with human se-rum albumin

Authors:
Yali Wu, Lili Chen, Jian Chen, Hao Xue, Qingfeng He, Dafang Zhong, Xingxing Diao

Article number: DMD-AR-2022-001019

Supp. Fig.1 The structures of 1H and 13C of furmonertinib and furmonertinib-lysine

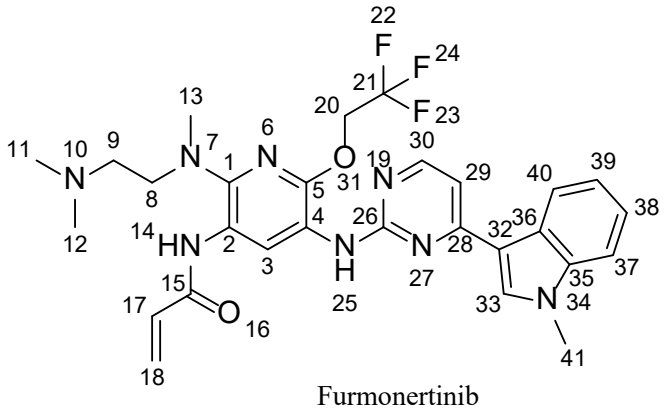

Furmonertinib

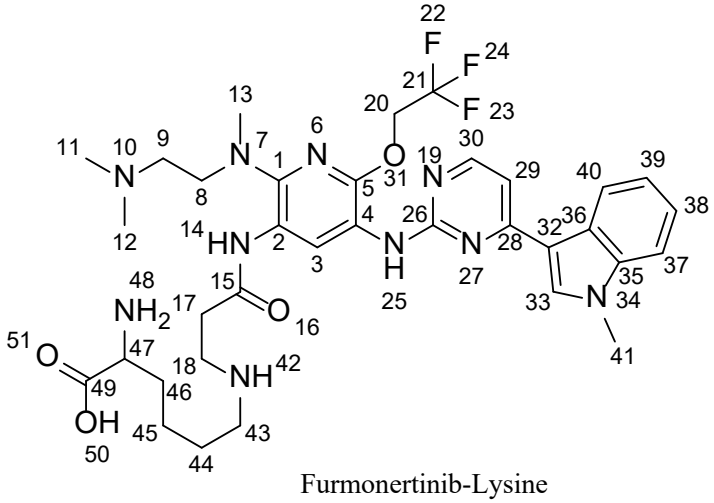

Furmonertinib-Lysine

Supp. Table 1 The chemical shifts of 1H and 13C of furmonertinib and furmonertinib-lysine

	Furmonertinib-Lysine		Furmonertinib
Atom	$^{13}C\ \delta$	$^{1}H\ \delta$	$^{1}H\ \delta$
1	147		
3	131.5	8.54	8.41
5	148.24		
8	51.36	3.3	
9	55.69	2.62	
11,12	44	2.35	2.85
13		2.84	2.8
17	43.27	3.05	6.59
18	47.39	2.75	6.34,5.83
20		4.96	5.01
28	161.64		
29	107	7.16	7.16
30	157.18/121.65	8.24	8.28
32	112.82		
33	133.4	8.39	8.41
35	137.97		
37	164.67	8.32	8.28
38	121.98	7.24	7.24
39	120.79	7.12	7.12
40	110.43	7.51	7.52
41		3.88	3.88
43	47.12	2.77	
44	26.68	1.54	
45	22.21	1.4	
46	30.34	1.67	
47	53.75	3.24	

Supp. Fig.2. The MS2 spectra of furmonertinib and synthesized furmonertinib-lysine adducts and the fragmentation pathways

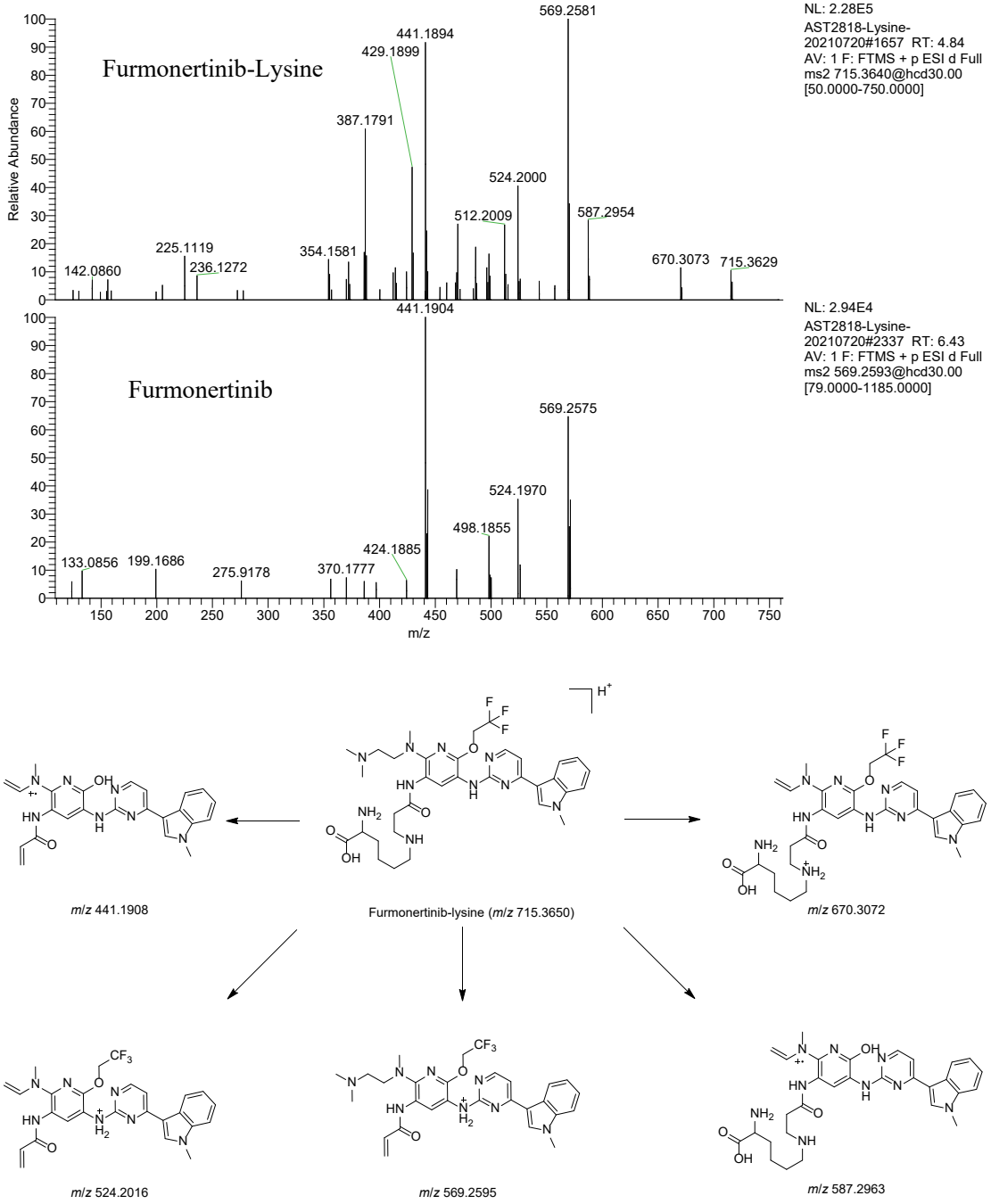

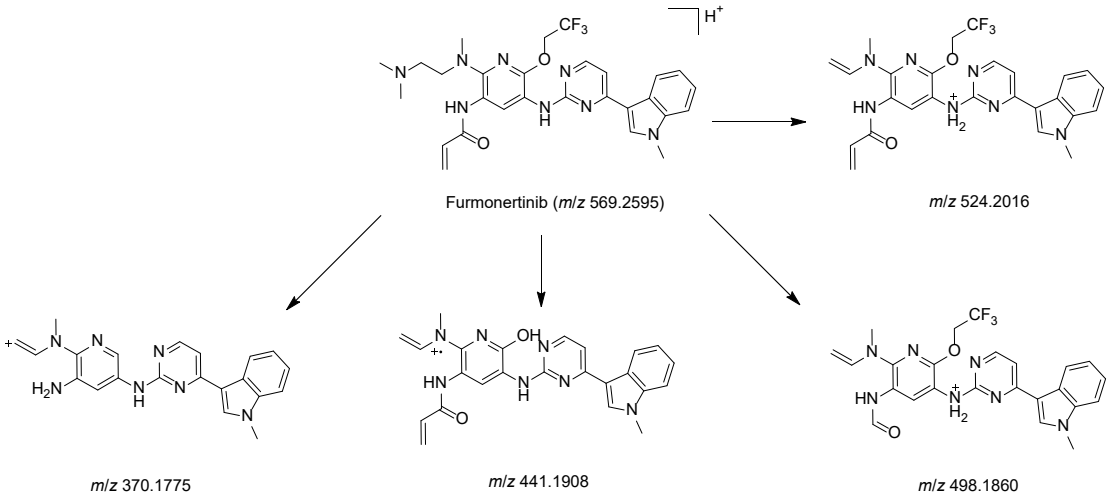
Furmonertinib (m/z 569.2595)
m/z 524.2016
m/z 370.1775
m/z 441.1908
m/z 498.1860

Supp. Fig.3 XIC of furmonertinib-lysine adduct in pronase digested sample (a) and spiked with synthetic standard (b)

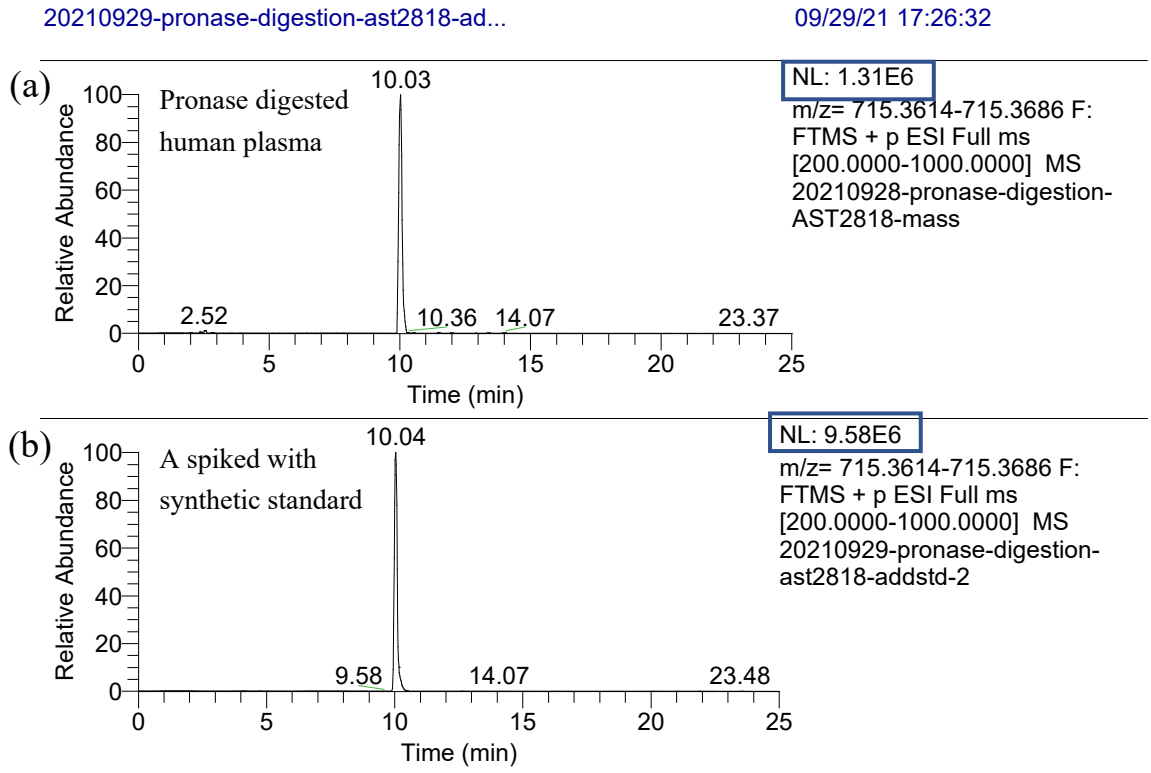

Supp. Fig.4 Structural identification of furmonertinib-MKCSSMQR adducts (a) and furmonertinib- MKCSSMQR adducts (b)

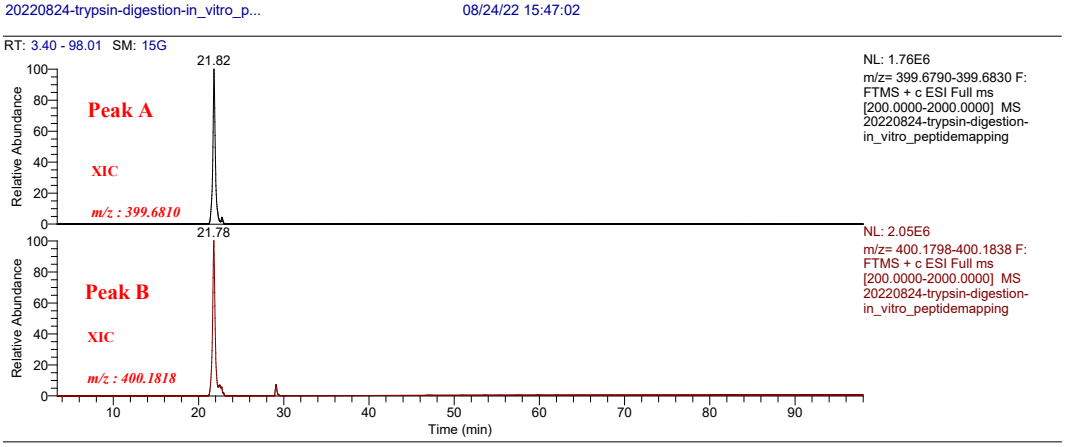

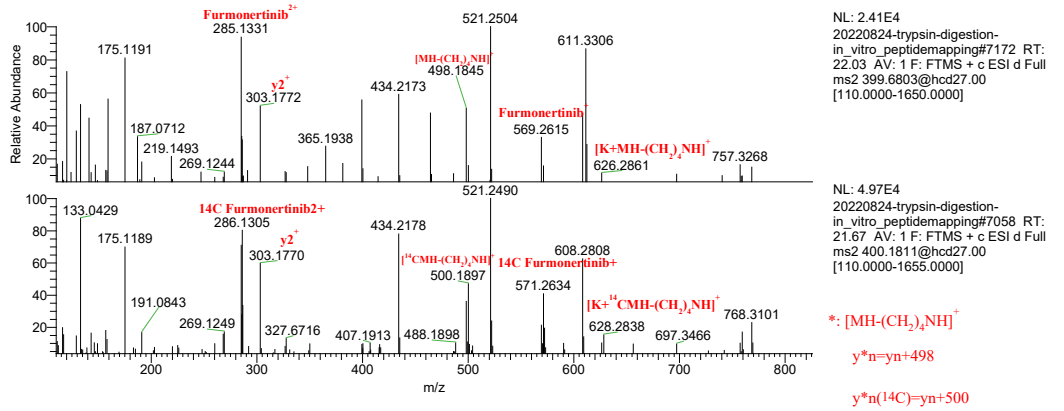

*: $[MH-(CH_2)_4NH]^+$

y*n=yn+498

y*n(^{14}C)=yn+500

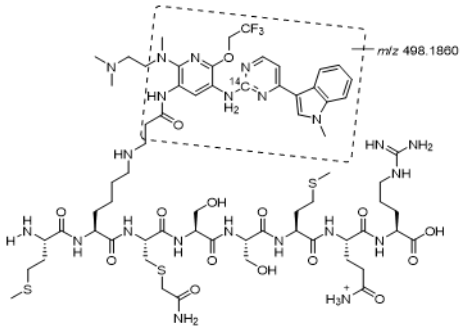

C12 furmonertinib-MKCSSMQR			
1H	2H	3H	4H
1595.7004	798.3541	532.5720	399.6810
1H	2H	3H	4H
C14 furmonertinib-MKCSSMQR			
1597.7036	799.3557	533.2398	400.1818